ROYAL SOCIETY OF CHEMISTRY

EDGE ARTICLE

Check for updates

Targeted regulation and optimization of multifunctional phase transition materials by novel void occupancy engineering†

Zhi-Jie Wang, [a] Hao-Fei Ni, [b] Tie Zhang, [a] Jie Li, [a] Meng-Meng Lun, [a] Da-Wei Fu [a] *[a] Zhi-Xu Zhang *[b] and Yi Zhang *[b]

As an innovative form of stimulus-response materials, organic–inorganic hybrid phase transition materials have become a wonderful contender in the field of functional electronic equipment due to their versatile structure, intensive functions and straightforward preparation. However, the targeted regulation and optimization of the electrical/optical response, along with the establishment of regular structure–performance relationships, pose significant challenges in meeting the diverse demands of practical applications over an extended period. Herein, we conducted a systematic investigation into the role of lattice void occupancy in regulating phase transition temperature (T_p) and related optical/electrical bistability. By taking hybrid material [TMEA][Cd(SCN)$_3$] featuring a flexible ammonium cation [TMEA]$^+$ (TMEA = ethyltrimethylammonium) as the prototype, we successfully synthesized three phase transition materials, namely [DEDMA][Cd(SCN)$_3$], [TEMA][Cd(SCN)$_3$] and [TEA][Cd(SCN)$_3$] (DEDMA = diethyldimethylammonium, TEMA = triethylmethylammonium, and TEA = tetraethylammonium), and the excellent regulation of the physical properties of these compounds was achieved through subtle engineering of void occupancy. More strikingly, [TEA][Cd(SCN)$_3$] exhibits remarkable bistable properties in terms of dielectric and nonlinear optical responses (with second-harmonic generation intensity reaching 2.5 times that of KDP). This work provides a feasible avenue to reasonably customise organic–inorganic hybrid phase transition materials and finely adjust their intriguing functionalities.

Introduction

Organic–inorganic hybrid phase transition materials exhibit reversible conversion between at least two distinct states in response to external stimulation, rendering them a novel class of multifunctional materials.[1–8] They have a wide range of applications in data storage, photoelectric detection and data communication due to their capability of integrating the strengths of inorganic and organic components.[9–17] However, exploring targeted chemical design methods has continuously been a crucial aspect in the construction of phase transition materials with desirable functionalities. Another essential and challenging issue that warrants in-depth exploration is the targeted regulation and optimization of multifunctional phase

transitions through exploiting specific structure–property relationships.

In recent years, significant progress has been made in the design and regulation of molecular-based phase transition materials.[18–33] It is worth noting that the "quasi-spherical theory" aims to reduce molecular symmetry and generate oriented molecular dipole moment by introducing specific chemical groups into spherical cations, which is expected to produce a low-symmetric polar crystal structure and even exhibit ferroelectric phase transition behavior.[34,35] Hua *et al.* modified the [(CH$_3$)$_4$N]$^+$ cation with a halogen (F, Cl, Br, and I) to enhance the phase transition temperature and successfully obtained a hybrid perovskite ferroelectric [(CH$_3$)$_3$NCH$_2$I]PbI$_3$.[36] Zhang *et al.* synthesized MeHdabco (*N*-methyl-1,4-diazoniabicyclo[2.2.2]octane) with molecular dipole moments by introducing methyl groups to break the mirror plane of DABCO (1,4-diazabicyclo[2.2.2]octane) molecules and successfully fabricated a 3D perovskite structure ferroelectric [MeHdabco]RbI$_3$.[37] Although modifying spherical molecules to quasi-spherical molecules can significantly lower crystal symmetry, precisely triggering a low-symmetric polar crystal structure remains challenging.

Void occupancy refers to the ratio of the void volume available for accommodating organic cations between inorganic anions, to the volume of a unit cell. The slight variation in lattice void occupancy will cause significant differences in the

[a] Ordered Matter Science Research Center, Jiangsu Key Laboratory for Science and Applications of Molecular Ferroelectrics, Southeast University, Nanjing 211189, People's Republic of China. E-mail: dawei@seu.edu.cn

[b] Institute for Science and Applications of Molecular Ferroelectrics, Key Laboratory of the Ministry of Education for Advanced Catalysis Materials, Zhejiang Normal University, Jinhua 321004, People's Republic of China. E-mail: zhangzhixu@zjnu.edu.cn; yizhang1980@seu.edu.cn
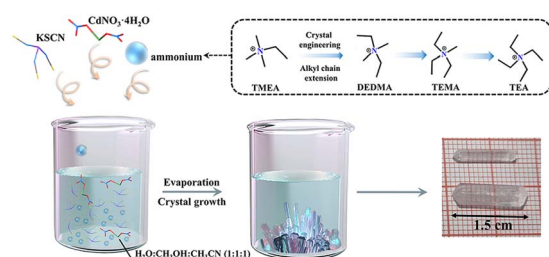
properties of phase transition materials, enabling us to systematically investigate and design these materials with precision.[38,39] Therefore, is it feasible to discover a hybrid system that exhibits a specific correlation between its organic and inorganic components, facilitating precise regulation of the crystal structure and properties, thereby enabling deeper exploration of the structure–property relationship? In an organic–inorganic hybrid system utilizing cadmium thiocyanate as the inorganic framework, the cations are arranged within the infinite polymer $[Cd(SCN)_3]_n^-$ inter-chain void, forming a highly compact arrangement.[40] The cations in such hybrid systems play multiple roles as organic spacers and controllers, which can generate various fascinating structures based on their size, shape, symmetry and charge.[41] Thus, it is worthwhile to investigate the ingenious regulation of lattice void occupancy through crystal engineering to achieve crystal polarity and modulation of phase transitions in such systems.

Inspired by the aforementioned research strategy, we selected $[TMEA]^+$ as a prototype cation for exploring void occupancy, as illustrated in Scheme 1. Three novel one-dimensional hybrid phase transition materials have been successfully synthesized based on three larger-sized quasi-spherical molecules, namely DEDMA, TEMA, and TEA, which were obtained by sequentially extending the methyl group of $[TMEA]^+$ to ethyl. The phase transition temperatures of these materials show a gradual upward trend, prompting us to further investigate the correlation between void occupancy and phase transition temperature. More encouragingly, it has been successfully demonstrated that the manipulation of void occupancy enables the construction of high-temperature phase transition materials. Simultaneously, the adoption of crystal engineering regulations *via* alkyl extension triggers a transformation in the crystal structure from centrosymmetric to polar, resulting in $[TEA][Cd(SCN)_3]$ exhibiting prominent nonlinear optical and dielectric bistable state response properties. This systematic molecular design work based on void occupancy will provide new insights into the exploration of organic–inorganic hybrid phase transition materials.

Results and discussion

Thermal analysis

The colorless rod-shaped crystals of the four compounds were obtained through the solution method (Fig. S1†), and their

purity was first studied through powder X-ray diffraction (PXRD) (Fig. S2†). The obtained PXRD patterns, which are closely consistent with the patterns generated by simulating single-crystal formations at ambient temperature (Fig. S3†), indicate the high purity of the corresponding phases. Besides, infrared spectroscopy further confirms the structural composition and functional group information of the compounds. The peaks located at 2100 and 760 cm^{-1} belong to the characteristic absorption peaks of SCN in the compounds, and ν_{C-H} (2975 and 2810 cm^{-1}), δ_{C-H} (1460 cm^{-1}), and ν_{C-N} (1190 cm^{-1}) are assigned to the absorption of ammonium cations. As a direct and trustworthy thermodynamic analysis technique, differential scanning calorimetry (DSC) is employed in solid-state phase transition research to record the T_p and study its thermodynamic process by measuring the heat change throughout the temperature shift. As illustrated in Fig. S4,† $[TMEA][Cd(SCN)_3]$ showed no noticeable reversible phase transition behaviour during the heating–cooling cycles from 153 K to 423 K. As depicted in Fig. 1, the extension of methyl groups in $[TMEA]^+$ to ethyl chains resulted in three quasi-spherical molecules, namely DEDMA, TEMA and TEA, exhibiting reversible phase transition behaviours with sequential increasing temperature at 333/316 K (T_{p1}), 342/323 K (T_{p2}) and 375/358 K (T_{p3}), respectively. These transitions were accompanied by significant thermal hysteresis observed at 16, 19 and 17 K, respectively. For concision, the phase below the phase transition is designated as the room-temperature phase (RTP), while the one above T_p is denoted as the high-temperature phase (HTP). Additionally, the three compounds showed obvious enthalpy changes (ΔH) of 6.21, 16.12 and 17.14 kJ mol^{-1}, respectively, during the phase transition from the RTP to the HTP. Then, the entropy changes (ΔS) were calculated to be 19.18, 48.38 and 46.68 J mol^{-1} K^{-1}, respectively, by combining with the equation $\Delta S = \Delta H/T$ demonstrating that the phase transition resulted in intrinsic structural alterations.

Crystal structure analysis

To comprehend the impact of alkyl chain extension on the organic–inorganic hybrid materials, the single crystal structures of $[TMEA][Cd(SCN)_3]$, $[DEDMA][Cd(SCN)_3]$, $[TEMA][Cd(SCN)_3]$

Scheme 1 The design concept of void occupancy engineering and the experimental process.

Fig. 1 DSC curves of $[DEDMA][Cd(SCN)_3]$, $[TEMA][Cd(SCN)_3]$, and $[TEA][Cd(SCN)_3]$ during heating–cooling cycles.

and [TEA][Cd(SCN)$_3$] were measured in different states. In terms of structure, all four compounds feature a 1D ABX$_3$ perovskite structure, wherein ammonium cations occupy the voids between the infinite [Cd(SCN)$_3$]$^-$ chains. At 298 K, [TMEA][Cd(SCN)$_3$] crystallizes in the centrosymmetric space group $P2_1/c$ (No. 14, point group $2/m$) of the monoclinic system. The cell parameters of [TMEA][Cd(SCN)$_3$] at 293 K are as follows: $a = 9.3109(7)$ Å, $b = 10.7164(6)$ Å, $c = 14.9364(11)$ Å, $\beta = 90.634(7)°$, $V = 1490.25(18)$ Å^3 and $Z = 6$ (Fig. S5†). As Fig. 2 displays, [DEDMA][Cd(SCN)$_3$], [TEMA][Cd(SCN)$_3$] and [TEA][Cd(SCN)$_3$] crystallizes in the space groups $Pnma$ (No. 62, point group mmm), $P2_1/c$ (No. 14, point group $2/m$) and $Cmc2_1$ (No. 36, point group $mm2$), respectively, and the detailed crystal data are listed in Tables S1–S4.† For compound [DEDMA][Cd(SCN)$_3$], partial disorder is observed in the ammonium cations in the RTP, with greater intensity of methyl disorder (Fig. S6†). For compound [TEMA][Cd(SCN)$_3$], its smallest asymmetric unit is composed of a molecular formula unit [TEMA][Cd(SCN)$_3$], with all atoms in the general position and completely ordered (Fig. S6†).

In the RTP, the anionic cadmium thiocyanate polymer chain is configured in a zigzag Cd⋯Cd⋯Cd pattern. For the inorganic chains of [DEDMA][Cd(SCN)$_3$] and [TEMA][Cd(SCN)$_3$], three S and three N atoms from six SCN$^-$ ligands are bonded to one Cd atom to form a twisted octahedron and triple bridged one-dimensional chain. The Cd–N bond distances in the [DEDMA][Cd(SCN)$_3$] and [TEMA][Cd(SCN)$_3$] range from 2.271(8) Å to 2.376(7) Å for [DEDMA][Cd(SCN)$_3$], and 2.282(6) Å to 2.349(6) Å for [TEMA][Cd(SCN)$_3$]. The Cd–S bond distances of [DEDMA][Cd(SCN)$_3$] and [TEMA][Cd(SCN)$_3$] range from 2.704(3) to 2.756(2) Å and from 2.7339(19) to 2.762(2) Å, respectively. The bond angle values of the –[N–C–S]– chains of [DEDMA]

[Cd(SCN)$_3$] and [TEMA][Cd(SCN)$_3$] are from 175.9(7)° to 178.6(8)° for [DEDMA][Cd(SCN)$_3$] and from 177.7(6)° to 178.9(6)° for [TEMA][Cd(SCN)$_3$], which is close to the 180° arrangement. The bond lengths and bond angles of [DEDMA][Cd(SCN)$_3$] and [TEMA][Cd(SCN)$_3$] are comparable to those observed in previously reported thiocyanate compounds. The adjacent chains based on TMEA, DEDMA, and TEMA cations are arranged in an "antiparallel" manner to each other and traverse the 2-fold screw axis, as shown in Fig. 3a and S8.† Additionally, the inter-chain void is occupied by ammonium cations.

The formation of large quasi-spherical [TEA]$^+$ cations occurs when all methyl groups in [TMEA]$^+$ are elongated into ethyl chains. The crystal parameters of [TEA][Cd(SCN)$_3$] that we synthesized are consistent with those reported previously in the literature.[42,43] It is worth noting that the anionic cadmium thiocyanate chain shows a perfectly parallel arrangement as the ammonium cation changes to [TEA]$^+$ (Fig. 3b), which highlights the impact of cation control on the inorganic [Cd(SCN)$_3$]$^-$ chains.

In the HTP, as shown in Fig. 2, three compounds belong to the same centrosymmetric space group $P6_3/mmc$ (No. 194, point group $6/mmm$). The [DEMA]$^+$, [TEMA]$^+$ and [TEA]$^+$ cations are situated at the symmetrical position of $6/mmm$, showing analogous disordered orientation or movement patterns. We thus model the cations as a spherical-like shape to meet their highly
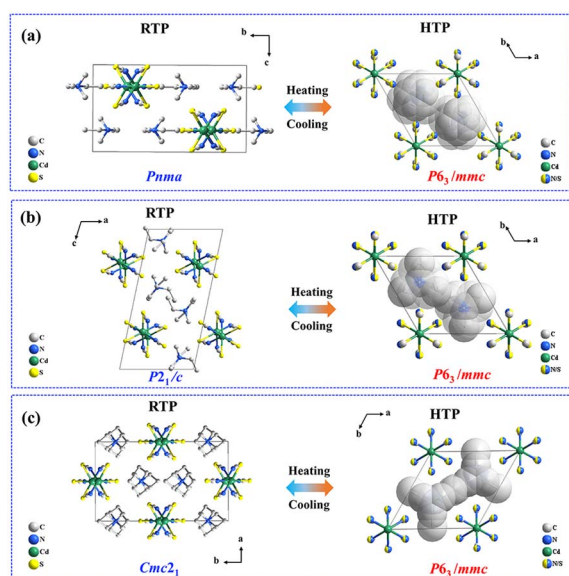

Fig. 2 (a) Crystal packing structures of [DEDMA][Cd(SCN)$_3$] in the RTP and HTP are compared. (b) Crystal packing structures of [TEMA][Cd(SCN)$_3$] in the RTP and HTP are compared. (c) Crystal packing structures of [TEA][Cd(SCN)$_3$] in the RTP and HTP are compared. Hydrogen atoms were omitted for clarity.
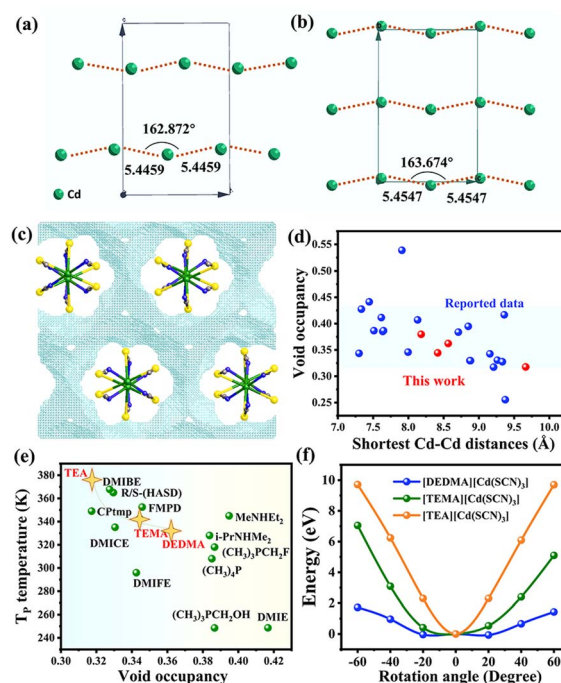

Fig. 3 Cd–Cd–Cd anion chain arrangement in [TEMA][Cd(SCN)$_3$] (a) and [TEA][Cd(SCN)$_3$] (b). (c) The void profile between [Cd(SCN)$_3$]$^-$ chains (cations are omitted for calculation). (d) Correlation between Cd–Cd distances and void occupancy based on our experimental results and the literature reported. (e) Relationship between void occupancy and phase transition temperature (compounds details can be seen in the ESI†). (f) The energy barrier of cations in the three compounds at different rotations (from −60° to 60°).

6-fold disorder states. The inorganic part of the $[Cd(SCN)_3]^-$ chain also exhibited disorder, with unidentified specific positions for the N and S atoms of the SCN^- anion. Therefore, the N and S atoms in the HTP were refined as a same-site to model a disordered state, and the $[Cd(SCN)_3]^-$ chain showed an infinitely long regular zigzag chain. However, cadmium atoms relocated with increasing temperature, resulting in the formation of a more regular linear Cd···Cd···Cd chain structure compared to that observed in the RTP. To sum up, the microstructure manifests that the temperature-induced structural phase transition belongs to the order–disorder type phase transition.

Relationship between void occupancy and phase transition

In such organic–inorganic hybrid systems, the arrangement of chains can be influenced by charge-balanced cations filling the inter-chain space, resulting in varying void volumes between $[Cd(SCN)_3]^-$ chains to accommodate these cations.[41] The differences in the inter-chain distance, void volume and the phase transition temperature require us to further investigate the literature to seek a deeper understanding of how void volume affects cation motion and phase transition. We extracted structural information obtained from the reported 1D organic–inorganic hybrid structures containing cadmium thiocyanate and integrated it with external data to generate relevant charts (Fig. 3d, e, Tables S5 and S7†). To evaluate the void volume between chains appropriately, we introduced the concept of void occupancy, which is determined from the void volume occupied in each unit cell after removing the cations compared to the total volume per unit cell and can be calculated by the OLEX2 software. It is evident that despite variations in the shortest $[Cd(SCN)_3]^-$ distance, as measured by the distance between Cd atoms between chains, the void occupancy remains relatively consistent at 30% to 45%, reflecting a stable structure resulting from interactions between the inorganic anion $[Cd(SCN)_3]^-$ chain and the cations. The correlation between void occupancy and phase transition temperature reveals a remarkable trend in all reported hybrid phase transition materials, wherein the phase transition temperature increases as the void occupancy decreases. This stems from the fact that cations face larger energy barriers when undergoing order–disorder conformational transitions within tightly arranged inter-chains. For example, He *et al.* substituted $[DMIFE]^+$ cations with halogens, resulting in a decrease in void occupancy from 41.67% to 32.75%, accompanied by a significant increase in the corresponding phase transition temperature.[40] In our research, we regulated alkyl chain extended quasi-spherical cations to alter void occupancy from 37.96% to 31.76%, obtaining a compound $[TEA][Cd(SCN)_3]$ with the highest phase transition temperature of 375 K as currently reported (Fig. S7†). Density functional theory (DFT) calculations have been applied to deeply investigate the T_p enhancement mechanism and steric hindrance effect of crystal engineering regulation on the three newly obtained phase transition materials. The computational models depicting the rotational energy barriers of the three compounds are shown in Fig. S12–S14.† In the theoretical

calculations of the model, the energy of the system at different rotation angles is influenced by intermolecular interactions, steric hindrance, and cation size and mass, leading to distinct phase transition temperatures.[44] The energy barrier of cations in the three compounds at different rotation angles show a trend of TEA > TEMA > DEDMA (Fig. 3f and Table S6†), which is consistent with the correlation between void occupancy and T_p analyzed structurally. Therefore, the introduction of extended alkyl groups enhances the energy barrier of motion and the steric resistance, facilitating an improvement in the phase transition temperature.

Dielectric properties

The solid–solid phase transition behaviours usually lead to anomalous alterations in electrical characteristics such as dielectric constants.[45,46] As demonstrated in Fig. 4a–c and S9,† the three compounds show dielectric anomalies at 333, 342 and 375 K, respectively, accompanied by a step-like dielectric switching behaviour from a low to a high dielectric state. It is worth noting that the anomaly change in the dielectric constant ($\Delta\varepsilon'$) during the phase transition process of $[TEA][Cd(SCN)_3]$ is significantly greater than that of $[DEDMA][Cd(SCN)_3]$ and $[TEMA][Cd(SCN)_3]$, which can be attributed to the inherent dipole of the polar structure. Under an external electric field, the phase transition from polarity to a centrosymmetric structure is accompanied by the disappearance of the dipole, resulting in a larger dielectric constant jump. As shown in Fig. S10,† the permittivity curves of the three compounds at different frequencies still show large dielectric anomalies around the T_p. The aforementioned results are perfectly compatible with the DSC observations. Furthermore, $[TEA][Cd(SCN)_3]$ was selected as a representative compound for further investigation into the properties of switchable dielectrics, as depicted in Fig. 4b. The switchable dielectric signal demonstrates excellent reversibility and fatigue resistance, reflecting no decay in increasing

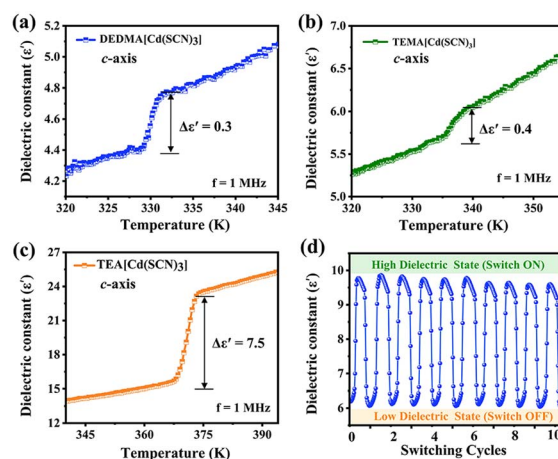**Fig. 4** Temperature dependence of the real part of the complex dielectric constant along the *c*-axis of $[DEDMA][Cd(SCN)_3]$ (a), $[TEMA][Cd(SCN)_3]$ (b), and $[TEA][Cd(SCN)_3]$ (c) single crystal samples at 1 MHz. (d) Temperature response of $[TEA][Cd(SCN)_3]$ to a dielectric bistable cycle at 1 MHz.

measurement time even after repeated heating and cooling between a high dielectric state and a low dielectric state within the temperature range of 355 K to 380 K for ten cycles. This indicates that these compounds possess the potential to serve as exceptional candidates for thermally responsive dielectric switching materials.

Second harmonic generation (SHG)

Normally, the SHG response is exclusively observed in non-centrosymmetric materials or interfaces.[47–49] Due to the non-centrosymmetric structure in the RTP and centrosymmetric structure in the HTP (Fig. S11†), $[TEA][Cd(SCN)_3]$ is anticipated to become a solid NLO (nonlinear optical) switching material. We carried out SHG intensity measurement of the poly-crystalline powder of $[TEA][Cd(SCN)_3]$ using the Kurtz–Perry model ($\lambda = 1064$ nm, Nd:YAG pulsed laser). As illustrated in Fig. 5b and c, the SHG signal of $[TEA][Cd(SCN)_3]$ exhibits outstanding reversibility within the temperature range of 335–390 K with obvious step-like SHG signal changes. The detected SHG intensity in the RTP is approximately 2.5 times that of the KDP (Fig. 5a), corresponding to the high SHG state ("SHG-ON state"). When the temperature reaches 375 K, the SHG signal intensity declines abruptly from 2.5 times that of KDP to nearly zero (only noise error), which shows the low SHG state ("SHG-OFF state") in the HTP. This is consistent with the DSC-determined reversible phase transition at 375 K. The utilization of crystal engineering to assemble molecules in a specific manner and achieve dipole-parallel packing is an effective method for achieving polar crystal structures.[50] Compared to a similar high SHG intensity compound (i-PrNHMe$_2$) $[Cd(SCN)_3]$,[51] $[TEA][Cd(SCN)_3]$ also adopts a parallel arrangement of $[Cd(SCN)_3]^-$ chains (Fig. 5d). The parallel arrangement of dipole moments within a single chain generates a net dipole moment in the crystal, which is beneficial to engender efficient SHG properties,[42] while NLO switching characteristics arise from the structural phase transition from non-centrosymmetric to centrosymmetric.

Conclusions

In summary, this work indicates a significant correlation between the occupancy of voids in 1D organic–inorganic hybrid materials and the properties of phase transition materials. The reversible phase transitions of the three hybrid phase transition materials, namely $[DEDMA][Cd(SCN)_3]$, $[TEMA][Cd(SCN)_3]$, and $[TEA][Cd(SCN)_3]$ based on quasi-spherical molecules were successfully induced through crystal engineering, which were verified by DSC and dielectric measurement. SXRD revealed the order–disorder phase transition mechanism for the structural phase transition, which involves the cooperative interaction between organic cations and $[Cd(SCN)_3]^-$ anions. In addition, $[TEA][Cd(SCN)_3]$ exhibits bistable properties in terms of NLO and dielectric response. This work provides a novel viewpoint on the development of high-performance phase transition materials through void occupancy engineering.

Experimental

Materials

Ethyltrimethylammonium iodide (Macklin, 98%), diethyldimethylammonium hydroxide, 20 wt% solution in H_2O (HWRK Chem), triethylmethylammonium chloride (Alfa Aesar, 98%), tetraethylammonium chloride (Macklin, 98%), cadmium nitrate tetrahydrate (Aladdin, 99%), potassium thiocyanate (Macklin, 99%), hydrochloric acid (Sinopharm, 36–38%) and silver carbonate (Macklin, 99%) were used as received without further purification.

Characterization

Single crystal X-ray diffraction (SXRD), dielectric measurement, differential scanning calorimetry (DSC), powder X-ray diffraction (PXRD), infrared spectroscopy (IR) and second harmonic generation (SHG) are described elsewhere. Density functional theory (DFT) calculations, calculation methods and data are also shown in the ESI.† The ESI contains more information.†

Author contributions

Z.-J. W.: conceptualization, data curation, formal analysis, investigation, writing – original draft and writing – review & editing. H.-F. N.: data curation and formal analysis. T. Z.: conceptualization. J. L. and M.-M. L.: investigation and formal analysis. Z.-X. Z.: supervision and writing – review & editing. D.-W. F. and Y. Z.: supervision, funding acquisition, project administration and writing – review & editing.

Conflicts of interest

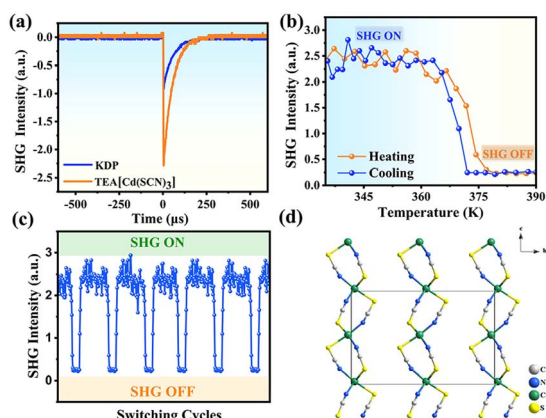The authors declare no conflict of interest.

Fig. 5 (a) SHG signal comparison of $[TEA][Cd(SCN)_3]$ and KDP at room temperature. (b) Temperature-dependent SHG intensity curve of $[TEA][Cd(SCN)_3]$ at 335–390 K. (c) Temperature response of $[TEA][Cd(SCN)_3]$ to an SHG bistable cycle (340–390 K). (d) Diagram of the parallel arrangement of $[Cd(SCN)_3]^-$ chains in $[TEA][Cd(SCN)_3]$.

Acknowledgements

Notes and references

1 B. Saparov and D. B. Mitzi, *Chem. Rev.*, 2016, **116**, 4558–4596.

2 W. Li, Z. Wang, F. Deschler, S. Gao, R. H. Friend and A. K. Cheetham, *Nat. Rev. Mater.*, 2017, **2**, 16099.

3 T. Zhang, K. Xu, J. Li, L. He, D.-W. Fu, Q. Ye and R.-G. Xiong, *Natl. Sci. Rev.*, 2023, **10**, nwac240.

4 M.-M. Lun, F.-L. Zhou, D.-W. Fu and Q. Ye, *J. Mater. Chem. C*, 2022, **10**, 11371–11378.

5 M. Mączka, J. K. Zaręba, A. Gągor, D. Stefańska, M. Ptak, K. Roleder, D. Kajewski, A. Soszyński, K. Fedoruk and A. Sieradzki, *Chem. Mater.*, 2021, **33**, 2331–2342.

6 J. Harada, Y. Kawamura, Y. Takahashi, Y. Uemura, T. Hasegawa, H. Taniguchi and K. Maruyama, *J. Am. Chem. Soc.*, 2019, **141**, 9349–9357.

7 Y. Ai, R. Sun, Y.-L. Zeng, J.-C. Liu, Y.-Y. Tang, B.-W. Wang, Z.-M. Wang, S. Gao and R.-G. Xiong, *Chem. Sci.*, 2021, **12**, 9742–9747.

8 Y.-K. Li, Y.-Y. Lai, T.-T. Ying, D.-C. Han, Y.-H. Tan, Y.-Z. Tang, P.-k. Du and H. Zhang, *Chem. Sci.*, 2021, **12**, 13061–13067.

9 Y. Wang, Z. Lv, L. Zhou, X. Chen, J. Chen, Y. Zhou, V. A. L. Roy and S.-T. Han, *J. Mater. Chem. C*, 2018, **6**, 1600–1617.

10 H.-Y. Hou, S. Tian, H.-R. Ge, J.-D. Chen, Y.-Q. Li and J.-X. Tang, *Adv. Funct. Mater.*, 2022, **32**, 2209324.

11 Y. Yao, H. Jiang, Y. Peng, X. Zhang, S. Chen, X. Liu and J. Luo, *J. Am. Chem. Soc.*, 2021, **143**, 15900–15906.

12 X. Zhang, T. Zhu, C. Ji, Y. Yao and J. Luo, *J. Am. Chem. Soc.*, 2021, **143**, 20802–20810.

13 T.-M. Guo, Y.-J. Gong, Z.-G. Li, Y.-M. Liu, W. Li, Z.-Y. Li and X.-H. Bu, *Small*, 2022, **18**, 2103829.

14 X.-G. Chen, X.-J. Song, Z.-X. Zhang, P.-F. Li, J.-Z. Ge, Y.-Y. Tang, J.-X. Gao, W.-Y. Zhang, D.-W. Fu, Y.-M. You and R.-G. Xiong, *J. Am. Chem. Soc.*, 2020, **142**, 1077–1082.

15 X.-J. Song, T. Zhang, Z.-X. Gu, Z.-X. Zhang, D.-W. Fu, X.-G. Chen, H.-Y. Zhang and R.-G. Xiong, *J. Am. Chem. Soc.*, 2021, **143**, 5091–5098.

16 J.-X. Gao, W.-Y. Zhang, Z.-G. Wu, Y.-X. Zheng and D.-W. Fu, *J. Am. Chem. Soc.*, 2020, **142**, 4756–4761.

17 Y. Chen, C. Gao, T. Yang, W. Li, H. Xu and Z. Sun, *Chin. J. Struct. Chem.*, 2022, **41**, 41313–41323.

18 C.-Y. Su, Y. Yao, Z. Zhang, Y. Wang, M. Chen, P.-Z. Huang, Y. Zhang, W. Qiao and D.-W. Fu, *Chem. Sci.*, 2022, **13**, 4794–4800.

19 H.-F. Ni, L.-K. Ye, P.-C. Zhuge, B.-L. Hu, J.-R. Lou, C.-Y. Su, Z. Zhang, L.-Y. Xie, D.-W. Fu and Y. Zhang, *Chem. Sci.*, 2023, **14**, 1781–1786.

20 D.-W. Fu, J.-X. Gao, P.-Z. Huang, R.-Y. Ren, T. Shao, L.-J. Han, J. Liu and J.-M. Gong, *Angew. Chem., Int. Ed.*, 2021, **60**, 8198–8202.

21 D.-W. Fu, J.-X. Gao, W.-H. He, X.-Q. Huang, Y.-H. Liu and Y. Ai, *Angew. Chem., Int. Ed.*, 2020, **59**, 17477–17481.

22 L.-P. Miao, N. Ding, N. Wang, C. Shi, H.-Y. Ye, L. Li, Y.-F. Yao, S. Dong and Y. Zhang, *Nat. Mater.*, 2022, **21**, 1158–1164.

23 Y. Takahashi, M. Takehisa, E. Tanaka, J. Harada, R. Kumai and T. Inabe, *J. Phys. Chem. Lett.*, 2020, **11**, 1336–1342.

24 R. Jakubas, M. Rok, K. Mencel, G. Bator and A. Piecha-Bisiorek, *Inorg. Chem. Front.*, 2020, **7**, 2107–2128.

25 Q. Jia, T. Shao, L. Tong, C. Su, D. Fu and H. Lu, *Chin. Chem. Lett.*, 2023, **34**, 107539.

26 J. Harada, M. Takehisa, Y. Kawamura, H. Takahashi and Y. Takahashi, *Adv. Electron. Mater.*, 2022, **8**, 2101415.

27 M. a. Mączka, M. Ptak, A. Gągor, D. Stefańska, J. K. Zaręba and A. Sieradzki, *Chem. Mater.*, 2020, **32**, 1667–1673.

28 M. Trzebiatowska, M. Mączka, A. Gagor and A. Sieradzki, *Inorg. Chem.*, 2020, **59**, 8855–8863.

29 M. Mączka, A. Nowok, J. K. Zaręba, D. Stefańska, A. Gągor, M. Trzebiatowska and A. Sieradzki, *ACS Appl. Mater. Interfaces*, 2022, **14**, 1460–1471.

30 J.-Y. Li, T. Zhang, M.-M. Lun, Y. Zhang, L.-Z. Chen and D.-W. Fu, *Small*, 2023, 2301364.

31 Y. Xie, Y. Ai, Y.-L. Zeng, W.-H. He, X.-Q. Huang, D.-W. Fu, J.-X. Gao, X.-G. Chen and Y.-Y. Tang, *J. Am. Chem. Soc.*, 2020, **142**, 12486–12492.

32 Y.-H. Fang, Z. Liu, S. Zhou, P.-X. Fu, Y.-X. Wang, Z.-Y. Wang, Z.-M. Wang, S. Gao and S.-D. Jiang, *J. Am. Chem. Soc.*, 2022, **144**, 8605–8612.

33 Y. Zhang, X.-J. Song, Z.-X. Zhang, D.-W. Fu and R.-G. Xiong, *Matter*, 2020, **2**, 697–710.

34 H.-Y. Liu, H.-Y. Zhang, X.-G. Chen and R.-G. Xiong, *J. Am. Chem. Soc.*, 2020, **142**, 15205–15218.

35 H.-Y. Zhang, Y.-Y. Tang, P.-P. Shi and R.-G. Xiong, *Acc. Chem. Res.*, 2019, **52**, 1928–1938.

36 X.-N. Hua, W.-Q. Liao, Y.-Y. Tang, P.-F. Li, P.-P. Shi, D. Zhao and R.-G. Xiong, *J. Am. Chem. Soc.*, 2018, **140**, 12296–12302.

37 W.-Y. Zhang, Y.-Y. Tang, P.-F. Li, P.-P. Shi, W.-Q. Liao, D.-W. Fu, H.-Y. Ye, Y. Zhang and R.-G. Xiong, *J. Am. Chem. Soc.*, 2017, **139**, 10897–10902.

38 C.-K. Yang, W.-N. Chen, Y.-T. Ding, J. Wang, Y. Rao, W.-Q. Liao, Y. Xie, W. Zou and R.-G. Xiong, *J. Am. Chem. Soc.*, 2019, **141**, 1781–1787.

39 G. R. Desiraju, *Angew. Chem., Int. Ed.*, 2007, **46**, 8342–8356.

40 L. He, L. Zhou, P.-P. Shi, Q. Ye and D.-W. Fu, *Chem. Mater.*, 2019, **31**, 10236–10242.

41 H. Zhang, X. Wang, K. Zhang and B. K. Teo, *Coord. Chem. Rev.*, 1999, **183**, 157–195.

42 H. Zhang, D. E. Zelmon, G. E. Price and B. K. Teo, *Inorg. Chem.*, 2000, **39**, 1868–1873.

43 M. Taniguchi and A. Ouchi, *Bull. Chem. Soc. Jpn.*, 1989, **62**, 424–428.

44 Z.-S. Yao, H. Guan, Y. Shiota, C.-T. He, X.-L. Wang, S.-Q. Wu, X. Zheng, S.-Q. Su, K. Yoshizawa, X. Kong, O. Sato and J. Tao, *Nat. Commun.*, 2019, **10**, 4805.

45 J. Ma, Q. Xu, L. Ye, Q. Wang, Z. Gong, C. Shi, H. Ye and Y. Zhang, *J. Rare Earths*, 2022, **40**, 937–941.

46 Y. Yu, P. Huang, Y. Wang, Z. Zhang, T. Zhang, Y. Zhang and D. Fu, *Chin. Chem. Lett.*, 2021, **32**, 3558–3561.

47 X. Chen and K. M. Ok, *Chem. Sci.*, 2022, **13**, 3942–3956.

48 P. Peksa, J. K. Zaręba, M. Ptak, M. a. Mączka, A. Gągor, S. Pawlus and A. Sieradzki, *J. Phys. Chem. C*, 2020, **124**, 18714–18723.

49 K. Ding, H. Ye, C. Su, Y.-A. Xiong, G. Du, Y.-M. You, Z.-X. Zhang, S. Dong, Y. Zhang and D.-W. Fu, *Nat. Commun.*, 2023, **14**, 2863.

50 R. Zhao, T. Zhu, S. Wang, C. Jarrett-Wilkins, A. M. Najjarian, A. J. Lough, S. Hoogland, E. H. Sargent and D. S. Seferos, *Chem. Sci.*, 2022, **13**, 12144–12148.

51 S.-Y. Zhang, X. Shu, Y. Zeng, Q.-Y. Liu, Z.-Y. Du, C.-T. He, W.-X. Zhang and X.-M. Chen, *Nat. Commun.*, 2020, **11**, 2752.